Inter- and Intraconfigurational Transitions of Nd 3+ in Hexafluoroelpasolite Lattices

ARTICLE *in* THE JOURNAL OF PHYSICAL CHEMISTRY B · JULY 2006

Impact Factor: 3.3 · DOI: 10.1021/jp0620320 · Source: PubMed

Inter- and Intraconfigurational Transitions of Nd^{3+} in Hexafluoroelpasolite Lattices

Peter A. Tanner,*,† Lixin Ning,† Vladimir N. Makhov,‡ Nicholas M. Khaidukov,§ and Marco Kirm||

Department of Biology and Chemistry, City University of Hong Kong, Tat Chee Avenue, Kowloon, Hong Kong S.A.R., People's Republic of China, Lebedev Physical Institute, Leninskii Prospect 53, Moscow 119991, Russia, Kurnakov Institute of General and Inorganic Chemistry, Leninskii Prospect 31, Moscow 119991, Russia, and Institute of Physics, University of Tartu, Riia 142, 51014 Tartu, Estonia

Received: April 2, 2006; In Final Form: April 27, 2006

Excitation of the $4f^3$ ion Nd^{3+} in hexafluoroelpasolite lattices by synchrotron radiation of wavelength ~185 nm leads to fast $4f^25d \rightarrow 4f^3$ emission below 52 630 cm^{-1} and slower $4f^3 \rightarrow 4f^3$ emission from the luminescent states $^4F_{3/2}$ Γ_{8u} (11 524 cm^{-1}) and $^2G(2)_{9/2}$ Γ_{8u} (~47 500 cm^{-1}). The near-infrared emission is well-resolved, and a clear interpretation of the $^4I_{9/2}$ crystal field levels and of the one-phonon vibronic sideband is given. The excitation spectrum of the $^2G(2)_{9/2}$ emission enables clarification of the structure of the $4f^25d$ configuration (which extends from ~52 000 to 128 000 cm^{-1}). Detailed energy level and intensity calculations have been performed, which provide simulations of the d−f emission and the f−d excitation spectra in good agreement with experiment. It is interesting that although the $4f^3$ $^2G(2)_{9/2}$ $\Gamma_{8u} \rightarrow 4f^3$ ^4I_J transitions are very weak in intensity compared with transitions terminating upon higher multiplet terms, most of the $4f^25d$ (^3H) $^4I_{9/2}$ $\Gamma_{8g} \rightarrow 4f^3$ emission intensity resides in the transitions to ^4I_J.

1. Introduction

The search for efficient phosphors and scintillators has been partly responsible for the recent upsurge in research concerning the interconfigurational transitions of lanthanide ions, Ln^{3+}.[1] The $4f^3$ ion Nd^{3+} has not been studied as widely as some other Ln^{3+}, but there have been reports of $4f^25d \rightarrow 4f^3$ emission for this ion doped into YPO_4.[2−5] In particular, fluoride hosts not only offer a wide band gap but the crystals are thermally stable and relatively inert compared with other halide hosts. Thus, most studies have focused upon the optical properties of Nd^{3+} in fluoride hosts, particularly in $LiYF_4$.[3,6−10] Under excitation by synchrotron radiation (SR), fast (nanosecond) $4f^25d \rightarrow 4f^3$ emission was observed from the luminescent state at 56 150 cm^{-1} (179 nm),[8] as well by upconversion under 351 nm excitation, when $4f^3 \rightarrow 4f^3$ emission was also observed.[6] The $4f^3 \rightarrow 4f^25d$ excitation spectra, which extend from ca. 55 000−80 000 cm^{-1} have also been experimentally recorded and simulated.[8,9] Collombet et al.[8,10] pointed out that the absorption maximum moves to higher $4f^25d$ energies when the initial $4f^3$ state moves to higher energy.

We have recently studied the $4f^3 \rightarrow 4f^3$ absorption and luminescence spectra of Nd^{3+} in $Cs_2NaNdCl_6$.[11] There is no $4f^25d \rightarrow 4f^3$ emission in this low-phonon host because the ladder of $4f^3$ levels overlaps the lowest $4f^25d$ state, which is then efficiently depopulated by nonradiative decay to give emission from the $^4D_{3/2}$ $4f^3$ multiplet term.[12]

In the present study, we revealed that both $4f^25d \rightarrow 4f^3$ and $4f^3 \rightarrow 4f^3$ emission can be observed under the excitation of Nd^{3+} in hexafluoroelpasolite hosts by SR. By contrast to the fluoride systems mentioned above,[3,6−10] the higher symmetry M_2ALnF_6 (M = Cs, Rb; A = Na, K; Ln = Y) elpasolite hosts utilized herein provide an octahedral (O_h) symmetry site for the Nd^{3+} to reside in so that strict optical transition site selection rules apply, which in some cases may limit the number of electric dipole allowed transitions and thereby simplify the spectra. We note that there have been relatively few previous studies of the d−f spectra of Ln^{3+} doped into hexafluoroelpasolite lattices. The SR excited emission spectra of Cs_2NaYF_6:Ln^{3+} (Ln = Tm, Er) have been reported,[13] and the spectra of the Tm system have been simulated.[14] The published spectra of the Ln = Ce system are not well-resolved.[15,16] Recently, a detailed experimental and theoretical study was performed for f^2 Pr^{3+} ions doped into Cs_2KYF_6.[17]

Following the experimental description (Section 2), the theoretical background of the energy level and intensity calculations is presented in Section 3. In the following Section 4, the $f^3 \rightarrow f^3$ emission spectra are presented and interpreted. The $f^2d \rightarrow f^3$ emission and $f^3 \rightarrow f^2d$ excitation spectra are then described and compared with the calculated transition intensities. Finally, in Section 5, the main conclusions of this work are listed.

2. Experimental Section

Chemical Preparation. The hydrothermal technique[18] was employed to synthesize single crystals of Nd^{3+}-doped hexafluoroelpasolites by using the blends of oxides $0.99Y_2O_3$−$0.01Nd_2O_3$ for Cs_2NaYF_6:Nd^{3+} (1 atom % Nd, hereafter abbreviated to 1%), Rb_2NaYF_6:Nd^{3+} (1%), and Cs_2KYF_6:Nd^{3+} (1%). These three double perovskites crystallize in the cubic O_h^5 space group with lattice parameters (in pm) 906.6 ± 1.0, 886.9 and 944.5, respectively.[19] The Nd^{3+} ion occupies a site of O_h symmetry in octahedral coordination geometry. For comparison, the layered perovskite $CsScF_4$:Nd^{3+} (0.5%) was also synthesized by using the blend of oxides $0.995Sc_2O_3$−$0.005Nd_2O_3$. This host lattice crystallizes in the space group D_{2h}^{13} below 317 K, with C_i site symmetry Nd^{3+} ions (ionic

* Corresponding author. E-mail: bhtan@cityu.edu.hk.
† City University of Hong Kong.
‡ Lebedev Physical Institute.
§ Kurnakov Institute of General and Inorganic Chemistry.
|| University of Tartu.

10.1021/jp0620320 CCC: $33.50
Published on Web 05/25/2006

radius 98 pm) substituting for Sc^{3+} (ionic radius 75 pm) in ScF_6^{3-} groups.[20]

Instrumentation. The studies of emission and excitation spectra were performed at the SUPERLUMI station[21] of HASYLAB at DESY (Hamburg) under pulsed excitation by SR in the range of 60−210 nm from the DORIS storage ring. Excitation spectra were typically recorded with an instrumental resolution of about 0.3 nm. Some excitation spectra were measured with a higher spectral resolution of 0.07 nm, but no additional features were found in the spectra as compared to the measurements with the lower spectral resolution. Luminescence spectra at room temperature and at 9 K in the UV, visible, and IR ranges were recorded with a 0.3 m Czerny−Turner-type secondary imaging monochromator-spectrograph SpectraPro-308i (Acton Research Corporation) equipped with a liquid-nitrogen-cooled CCD detector (Princeton Instruments, Inc.). The spectral resolution of the analyzing monochromator with the 300 lines/mm grating was set to ∼0.5 nm. One near-infrared emission spectrum of Cs_2NaYF_6:Nd^{3+} was recorded in high-resolution mode (∼5 times higher) by using the grating of 1200 grooves per mm. Excitation spectra of luminescence were recorded by a photomultiplier tube (Hamamatsu R6358P). Emission spectra in the VUV region were measured using a 0.5 m Pouey-type secondary VUV monochromator equipped with a solar-blind photomultiplier R6838 using an instrumental resolution of about 3 nm. All of the luminescence spectra were not corrected for the spectral response of the detection system. Time-resolved spectra were recorded with a time window of 40 ns for the fast component and 127 ns for the slow component, the latter window being delayed by 40 ns after the excitation pulse, which has duration of ∼150 ps. The crystals were cleaved before mounting onto the sample holder in a flow-type liquid helium cryostat. The crystallographic axes of the crystals when installed onto the sample holder were not oriented with respect to polarization vector of exciting radiation.

3. Energy Level and Intensity Calculations

Calculation of $4f^3$ and $4f^25d$ Energy Levels. The energy level calculation employed the extended f-shell programs of Prof. M. F. Reid, in which the electronic energy levels were calculated by simultaneous diagonalization of various parametrized Hamiltonians for $4f^3$ and $4f^25d$ configurations. The details of these calculations can be found in ref 9. In the calculation of $4f^3$ energy levels, parameter values for the interactions, including Coulomb interaction between the 4f electrons, the spin−orbit interaction, and the crystal-field interaction, were varied simultaneously within certain allowed ranges. The values of these parameters: F^2, ζ, B_0^4, and B_0^6 with fixed ratios F^4/F^2 and F^6/F^2, were optimized by repeatedly calculating $4f^3$ energy levels until the best agreement was obtained between the four calculated and observed crystal-field level energies. The four finally derived energies [calcd (exptl)] are from the spectrum of Cs_2NaYF_6:Nd^{3+}: 0 (0) cm^{-1}, 154.8 (155) cm^{-1}, 647.0 (647) cm^{-1}, and 11524.0 (11524) cm^{-1}, respectively. The resulting optimized parameter values are listed in Table 1, consistent with the trends for halide ligands (i.e., F and Cl) by comparison with the corresponding parameter values for $Cs_2NaNdCl_6$.[11] The values for the F^k ratios and other parameters of small free-ion interactions were taken from Nd^{3+} in LaF_3.[22] It has been established that the energies of certain $4f^3$ multiplet term crystal field levels are sensitive to the inclusion of configuration interaction with $4f^2np$.[11] This fine-tuning was not taken into account in the present calculations.

TABLE 1: Energy Parameters for the $4f^3$ and $4f^25d$ Configurations of Nd^{3+} in Cs_2NaYF_6[a]

$4f^3$		$4f^25d$	
parameter	cm^{-1}	parameter	cm^{-1}
F^2	72 188	ζ (d)	1216
F^4 [b]	52 625	B_0^4(d) [d]	38 220
F^6 [b]	35 372	Δ_E(fd)	50 901
ζ	871	F^2(fd)	22 626
α	[21.34]	F^4(fd)	11 205
β	[−593]	G^1(fd)	9787
γ	[1445]	G^3(fd)	8306
T^2	[298]	G^5(fd)	6437
T^3	[35]		
T^4	[59]		
T^6	[−285]		
T^7	[332]		
T^8	[305]		
M^0 [c]	[2.11]		
P^2 [c]	[192]		
B_0^4 [d]	3742		
B_0^6 [d]	452		

[a] For the $4f^3$ configuration, the values in brackets were not allowed to vary in the parameter optimization and taken from those of Nd^{3+} in LaF_3.[22] For the $4f^25d$ configuration, parameters for the splitting of the $4f^2$ core (not listed) are from the $4f^3$ configuration (and multiplied by 1.06 for free-ion parameters). The spin−orbit parameter for the 5d electron was obtained from ref 23, and the 5d crystal-field parameter from ref 16. Parameters for f−d interactions were calculated using Cowan's code[24] (but reduced by 26%). See ref 9 for parameter definitions. [b] The ratios, $F^4/F^2 = 0.729$ and $F^6/F^2 = 0.490$, are from ref 21. [c] $M = 0.56\,M^0$, $M^4 = 0.31\,M^0$; $P^4 = 0.75\,P^2$, $P^6 = 0.1\,P^2$. [d] The crystal-field Hamiltonians for the 4f and 5d electrons are defined as

$$H_{CF}(f) = B_0^4(f)[C_0^4 + (\sqrt{5}/\sqrt{14})(C_4^4 + C_{-4}^4)] + B_0^6(f)[C_0^6 - (\sqrt{7}/\sqrt{2})(C_4^6 + C_{-4}^6)]$$

and

$$H_{CF}(d) = B_0^4(d)[C_0^4 + (\sqrt{5}/\sqrt{14})(C_4^4 + C_{-4}^4)]$$

In the calculation of $4f^25d$ energy levels, parameter values for the interactions of the $4f^2$ core were taken from those of the $4f^3$ configuration, with those of free-ion multiplied by 1.06 to take into account the effect of a little more contracted 4f orbital in the $4f^2$ core in comparison with the $4f^3$ configuration.[23] For the 5d electron, the crystal-field parameter was calculated from the observed 5d crystal-field splitting of Ce^{3+} doped in Rb_2NaYF_6,[16] and the spin−orbit parameter was approximated by that of Nd^{3+} ($4f^25d$) in fluoride hosts.[23] The f−d interaction parameters were estimated from the standard atomic computer programs[24] but were reduced to 74% of the calculated free ion values.[23] In addition to the splitting into many energy levels due to interactions within the $4f^25d$ configuration, the position of the energy levels is determined by the difference between the average energies of $4f^25d$ and $4f^2$ configurations Δ_E(fd) because the energy levels of the two configurations are simultaneously calculated in the program. This energy difference comprises several sources, including kinetic energy, Coulomb and (isotropic) crystal field effects. The influence of Δ_E(fd) is to shift all of the $4f^25d$ energy levels by the same amount relative to the $4f^3$ ground state, and Δ_E(fd) is adjusted to obtain the best agreement between experiment and calculation. The energy parameters used in the calculation of the $4f^25d$ energy levels are collected in Table 1.

Calculation of $4f^3$−$4f^25d$ Transition Intensities. If we adopt the adiabatic approximation for the vibronically coupled system, then the unpolarized intensity I_{if} of the electronic transition from the initial $4f^3$ level $|f^3\Gamma_i\rangle$ to the final $4f^25d$ level $|f^2d\Gamma_f\rangle$ may be

expressed as

$$I_{if} \propto \bar{\nu}_{if} \sum_{q,\gamma_i,\gamma_f} |\langle f\,^3\Gamma_i\gamma_i|D_q^1|f\,^2d\Gamma_f\gamma_f\rangle|^2 |\langle\chi_i|\chi_f\rangle|^2 \quad (1)$$

where $\bar{\nu}_{if}$ is the vibronic transition wavenumber, D_q^1 is the electric dipole operator, χ_i and χ_f are the initial and final vibrational states, and the summation is over the polarization q ($q = 0, \pm 1$) and the components γ of the initial and final levels. In eq 1, the Condon approximation is also used in which the electronic transition moment is assumed to be independent of the vibrational wave functions.[25] If we assume that only the lowest vibrational level associated with the initial electronic state is populated, then the vibrational term on the right side of eq 1 can be given by

$$|\langle\chi_i|\chi_f\rangle|^2 = e^{-S}\frac{S^n}{n!} \quad (2)$$

where S is the Huang−Rhys factor and n is the vibrational quantum number of the terminal vibrational state. The expression for S can be obtained from an evaluation of the squared vibrational overlap integrals in eq 2 using the harmonic vibrational wave functions for the initial and terminal vibrational states, and can be written as

$$S = \frac{M\omega_i}{2\hbar}(\Delta Q_i)^2 \quad (3)$$

where M is the effective mass and ΔQ_i is the equilibrium displacement in the normal coordinate Q_i between the initial and final electronic states for the vibrational mode υ_i with the angular frequency ω_i.[25]

The transitions between $4f^3$ and $4f^25d$ states are electric dipole allowed. The electric dipole matrix elements in eq 1 can be calculated using the formulas described in ref 26 with the pure electronic wave functions obtained in the energy level calculations for $4f^3$ and $4f^25d$ configurations, and the squared vibrational overlap integrals can be calculated using the Huang−Rhys formulation as described above. To reproduce the observed excitation spectrum of $Cs_2NaYF_6:Nd^{3+}$ at the temperature of 9 K, Gaussian-shaped bands are superimposed on the calculated vibronic transition line, with the half width of 350 cm^{-1}, and with the intensity proportional to the calculated vibronic transition intensity. Only the totally symmetric a_{1g} vibrational mode for the NdF_6^{3-} moiety with the energy of 476 cm^{-1} [27] was employed in the simulation, with the Huang−Rhys factor $S = 1.2$.

In addition, we also calculated the $4f^25d \rightarrow 4f^3$ emission spectrum beginning at about 190 nm. The calculation procedure is the same as that for the $4f^3 \rightarrow 4f^25d$ excitation spectrum as described above, except that in eq 1 the initial and final electronic levels and vibrational states are now of $4f^25d$ and $4f^3$ configurations, respectively, with the factor $\bar{\nu}_{if}$ replaced by $\bar{\nu}_{if}^3$.

4. Results and Discussion

$4f^3-4f^3$ Emission Spectra. Under SR excitation (~185 nm; ~54 000 cm^{-1}), the $4f^25d$ levels of Nd^{3+} in elpasolite hosts are populated. Nonradiative decay and intersystem crossing to $4f^3$ levels can then occur, in addition to (fast) emission from the lowest $4f^25d$ level. The energy level calculation was employed to determine which $4f^3$ levels are potentially luminescent. It has been found in the absence of depopulation by energy transfer that a suitably populated energy level of Ln^{3+} in an elpasolite host lattice is potentially luminescent provided that the energy gap to the next lowest level is spanned by more than four phonons[28] (i.e., by >1880 cm^{-1} in the present case of $Cs_2NaYF_6:Nd^{3+}$ [27]). The calculated crystal field levels below 70 000 cm^{-1} that obey this criterion are listed Table 2, together with an additional one for which the energy gap is slightly less. Figure 1 emphasizes the congestion of the energy levels of Nd^{3+} in Cs_2NaYF_6, with the exception of these few gaps. Besides being higher than our excitation energy, the level at 65 540 cm^{-1} lies within the span of the $4f^25d$ configuration and is expected to depopulate to these states. This leaves only four potential $4f^3$ luminescence states for Nd^{3+} in the hexafluoroelpasolite hosts. Note that the lowest $^4G_{7/2}$ crystal field level is (weakly) luminescent in $Cs_2NaYCl_6:Nd^{3+}$. This level is calculated to be at 18 711 cm^{-1} in $Cs_2NaYF_6:Nd^{3+}$, but the energy gap to the next-lowest level is only 1037 cm^{-1}. Because it is spanned by only three phonons, luminescence is not expected in the present case. The gap below $^4D_{5/2}$ (which is calculated to be nearly equally mixed with $^4D_{3/2}$) is spanned by four phonons. A careful examination of the SR excited emission spectra shows no strong evidence for emission from $^2P_{3/2}$ and $^4D_{5/2}$, but emission is observed from the other two multiplets $^2G(2)_{9/2}$ and $^4F_{3/2}$ as described below. The absence of emission from $^2F(2)_{5/2}$ can readily be understood as due to a cross-relaxation process from $^2G(2)_{9/2}$, which competes with the radiative decay. For example, the process

$$^2G(2)_{9/2}\,(47\,560) + {}^4I_{9/2}\,(0) \rightarrow {}^2H(1)_{11/2}\,(34\,671) + {}^4F_{5/2}\,(12\,883)$$

where the energies of relevant crystal field levels are given in cm^{-1}, is calculated to be almost resonant and would feed $^4F_{3/2}$.

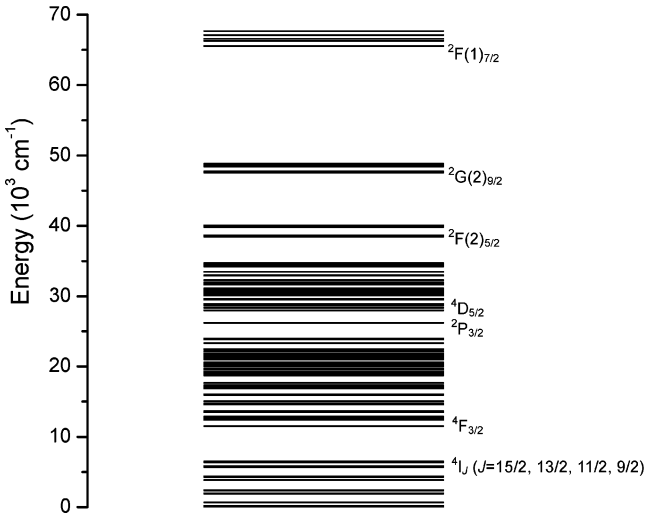

Figure 1. Calculated $4f^3$ energy levels of Nd^{3+} in the Cs_2NaYF_6 host. The multiplet terms listed in Table 2 are marked.

TABLE 2: Calculated $4f^3$ Energy Levels of Nd^{3+} in Cs_2NaYF_6 below 70 000 cm^{-1} that Have Appreciable Energy Gaps (>1500 cm^{-1}) from the Next Lower Levels

$^{2S+1}L_J$	Γ	energy (cm^{-1})	energy gap (cm^{-1})
$^2F(1)_{7/2}$	Γ_7	65 540	16 750
$^2G(2)_{9/2}$	Γ_8	47 560	7520
$^2F(2)_{5/2}$	Γ_8	38 453	3782
$^4D_{5/2}$	Γ_8	27 959	1758
$^2P_{3/2}$	Γ_8	26 201	2227
$^4F_{3/2}$	Γ_8	11 524	5064

Emission from $^4F_{3/2}$. We have recently reported the $^4F_{3/2} \rightarrow {}^4I_{9/2}$ emission transition in $Cs_2NaNdCl_6$[11] and the 10 K spectrum

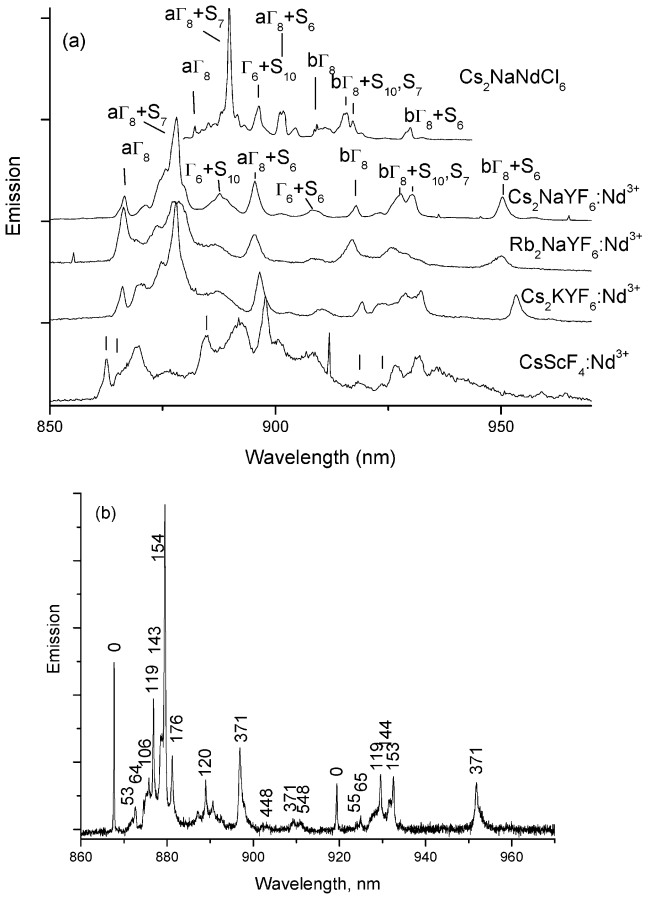

Figure 2. (a) Synchrotron radiation (174−188 nm) excited $^4F_{3/2} \rightarrow {}^4I_{9/2}$ emission spectra of Nd^{3+} in fluoride hosts at 9 K. The 355 nm excited spectrum of $Cs_2NaNdCl_6$ at 10 K is included for comparison. The initial state is $^4F_{3/2}$, and the terminal vibronic states are marked. (b) 188 nm excited high-resolution spectrum of $Cs_2NaYF_6:Nd^{3+}$ at 9 K. The vibronic displacements (cm^{-1}) from (inferred) zero phonon lines are marked.

is reproduced in Figure 2a to show the salient points for comparison with the present study. There are three crystal field levels of $^4I_{9/2}$ and the energies in $Cs_2NaNdCl_6$ are (in cm^{-1}): 0 $a\Gamma_8$, 97 Γ_6, and 335 $b\Gamma_8$. There is only one crystal field state (Γ_8) of the $^4F_{3/2}$ multiplet term. In this latter host the transition is mainly vibronic in character, Figure 2a, although the $\Gamma_8 \rightarrow a\Gamma_8$, $b\Gamma_8$ zero phonon lines are clearly observed. In the $\Gamma_8 \rightarrow a\Gamma_8$ sideband, S_7 (ν_4) is prominent, whereas S_{10} (ν_6) is prominent in the $\Gamma_8 \rightarrow \Gamma_6$ sideband (the vibrational notations refer to the unit cell group and $NdCl_6^{3-}$ moiety modes, respectively[27]). It is obvious in Figure 2a that the spectra of Nd^{3+} in the hexafluoroelpasolite hosts can be assigned in an analogous manner and the terminal vibronic states are marked in the figure. Figure 2b shows the low-temperature spectrum of Cs_2NaYF_6: Nd^{3+} under higher resolution and the vibronic displacements from the (inferred) zero phonon lines are marked. The $^4F_{3/2}$ energy is a little higher than that in $Cs_2NaNdCl_6$, reflecting greater Slater parameters, whereas the greater magnitudes of $^4I_{9/2}$ crystal field energy levels (by factors of 1.6 and 1.8) give greater crystal field parameters (by these similar ratios) in $Cs_2NaYF_6:Nd^{3+}$.

The derived vibrational energies for the hexafluoroelpasolite hosts are listed in Table 3 and are greater than those for Nd^{3+} in $Cs_2NaNdCl_6$ so that the spectra are more expansive than that of $Cs_2NaNdCl_6$ in Figure 2a. At 300 K, vibrational hot bands are clearly observed for the $\Gamma_8 \rightarrow a\Gamma_8$ transition. Notice that for the fluoride systems the band marked $\Gamma_6 + S_6$ has a long

TABLE 3: Derived Vibrational Energies from the $^4F_{3/2} \rightarrow {}^4I_{9/2}$ Emission Spectra of Nd^{3+} in Hexafluoroelpasolite Hosts

	derived vibrational energy (cm^{-1})			
host	S_9, S_5	S_6 (ν_3)[a]	S_7 (ν_4)	S_{10} (ν_6)
Cs_2NaYF_6	52, 67	377, 449	154	122
Rb_2NaYF_6	41, 54, 59	390 ± 2, 475	154 ± 3	115 ± 3
Cs_2KYF_6		376 ± 2	148 ± 7	98 ± 4

[a] Transverse and longitudinal optic modes.

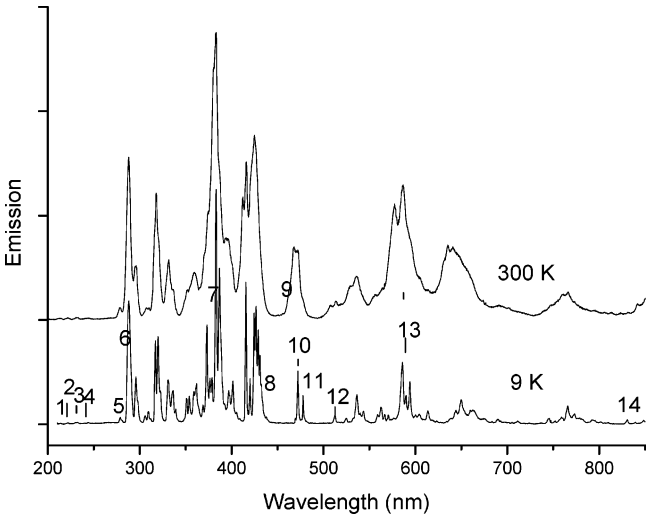

Figure 3. Room-temperature (λ_{exc} 180 nm) and 9 K (λ_{exc} 188 nm) emission spectra of $Cs_2NaYF_6:Nd^{3+}$. Refer to the text for a discussion of the numbered bands.

wavelength shoulder, which is not the case for $a\Gamma_8 + S_6$ or $b\Gamma_8 + S_6$. One assignment of this shoulder is to first member of the S_2 progression on the strong $a\Gamma_8 + S_7$ vibronic origin. The derived energies of S_2 are between 399 cm^{-1} (for Cs_2KYF_6) and 409 cm^{-1} (for Rb_2NaYF_6) and would indicate a weak, linear Jahn−Teller effect.

The lowest spectrum in Figure 2a corresponds to $CsScF_4$: Nd^{3+}, where the fourfold Kramers degeneracies of Γ_8 states are lifted. The assignments are very tentative in the absence of more detailed experiments. One possibility is shown in the figure, where zero phonon transitions are marked by lines, and vibrational intervals of 98 and 458 cm^{-1} are observed to be superimposed.

Emission from $^2G(2)_{9/2}$. The room-temperature and 9 K spectra of $Cs_2NaYF_6:Nd^{3+}$ under 188 nm excitation are compared in Figure 3. The higher energy bands are not well-resolved (fwhm ≈ 500 cm^{-1}) so that they comprise many overlapping vibronic features. Accurate energy level assignments are therefore not attempted, and it is sufficient to identify the multiplet term nature of the luminescent state(s) and terminal electronic states. To realize this, it is instructive to remember the large energy gaps between some of the terminal levels. For example, the gap between $^4F_{3/2}$ and $^4I_{15/2}$ is calculated to be 5064 cm^{-1}. This energy gap roughly matches that between bands 4 and 5, so that the weak features 1, 2, 3, and 4 (more visible in a slow emission component shown in Figure 5, see below) correspond to transitions to ^4I_J ($2J = 9, 11, 13, 15$), whereas band 5 represents the transition to $^4F_{3/2}$. Note that the next band (6) is more intense and the terminal level is $^4F_{5/2}$. Other big gaps between crystal field levels are those for $^2D(1)_{5/2} - {}^2P_{3/2}$ and $^2P_{3/2} - {}^4D_{5/2}$. Thus, line 8 represents the vibronic tail of the transition to $^2D(1)_{5/2}$, for lines 9−11 the terminal multiplet is $^2P_{3/2}$, and for line 12 it is $^4D_{5/2}$. The energy gaps are consistent with calculation. In fact, this region of the spectrum is rather

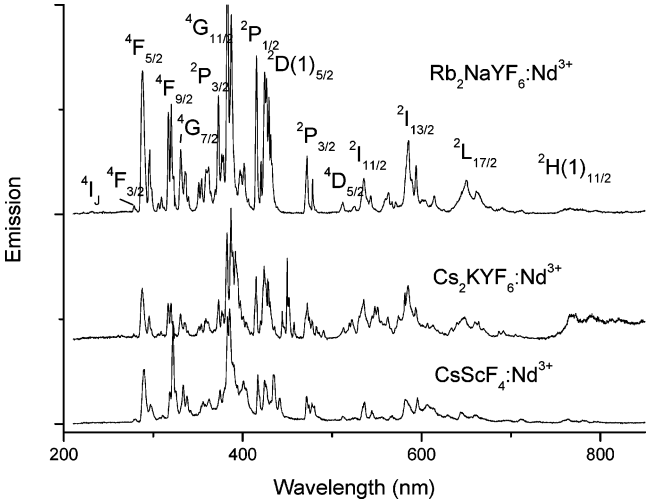

Figure 4. 9 K emission spectra of Nd^{3+} in fluoride hosts excited by synchrotron radiation (between 174 and 188 nm). The $4f^3$ luminescent state is $^2G(2)_{9/2}\ \Gamma_8$, and some of the terminal multiplet terms are marked.

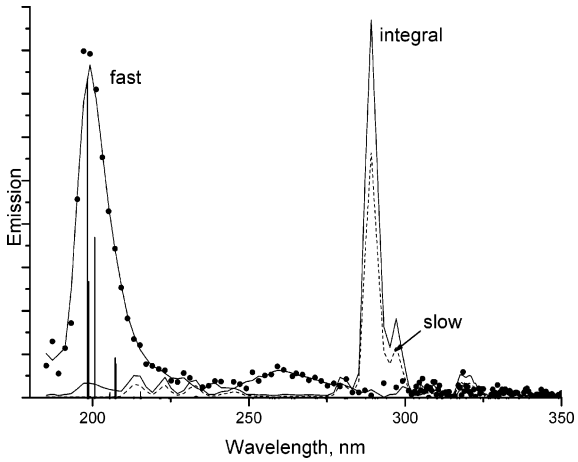

Figure 5. Time-resolved 180 nm excited emission spectra of $Cs_2NaYF_6:Nd^{3+}$ at 10 K. The fast (time window 40 ns) and slow (time window 127 ns: also delayed by 40 ns after the excitation pulse) components and the integral spectra are shown. The vertical bars are the calculated $4f^25d \rightarrow 4f^3$ emission intensities.

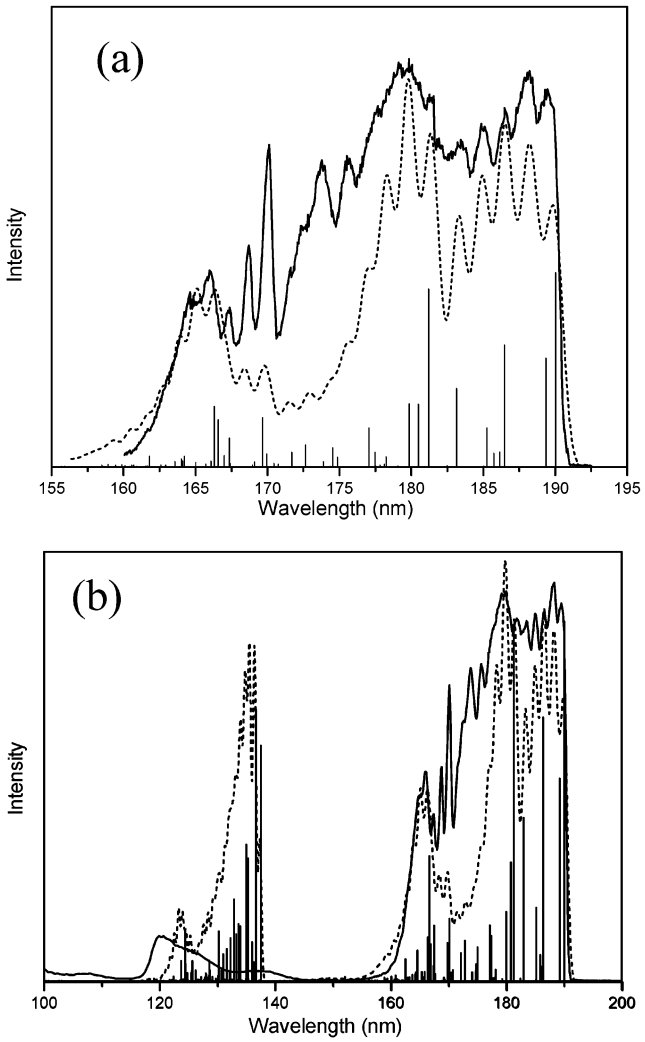

Figure 6. Experimental (9 K) and simulated excitation spectra for the $4f^3 \rightarrow 4f^25d$ transitions of Nd^{3+} in Cs_2NaYF_6. The solid curves are the experimental spectra with high resolution in the energy range of 160−193 nm in a and with lower resolution in the energy range of 100−200 nm in b. The vertical lines are the predicted positions of vibronic lines with heights proportional to predicted intensities, and the dashed curves are the simulated spectra.

more clearly resolved and the separation of 258 cm^{-1} between lines 10 and 11 enables them to be assigned to transitions terminating upon the $^2P_{3/2}$ S_{10} (122 cm^{-1}) and S_6 (377 cm^{-1}) vibronic structure. The corresponding S_{10} hot band is clearly visible as the shoulder, line 9 in the room-temperature spectrum. We do not perform detailed energy level assignments because of the energy level complexity of Nd^{3+} and the many overlapping transitions, which make interpretation ambiguous. From the analysis, however, it is possible to assign nearly all of the transitions to a luminescent state at 47 500 ± 500 cm^{-1}. From Table 2 this clearly corresponds to the $^2G(2)_{9/2}\Gamma_8$ state. The differences between the room-temperature and 9 K spectra are then attributed to emission from vibrationally excited levels of this state and those of the other crystal field levels of $^2G(2)_{9/2}$, which are calculated to be at 54 and 186 cm^{-1} to higher energy than $^2G(2)_{9/2}\Gamma_8$. In Figure 4, some of the terminal multiplet terms are marked for the corresponding emission spectra of the other systems studied. Note that the strong group of bands marked 13 in Figure 3 corresponds to the vibronic structure of the hypersensitive transition $^2G(2)_{9/2} \rightarrow {}^2I_{13/2}$.

A few weak lines in Figure 3 (e.g., line 14) cannot be associated with emission from $^2G(2)_{9/2}$. It is not possible to assign these conclusively. Alternative assignments of such bands are to emission from $^2P_{3/2}$ (calculated at 26 201 cm^{-1}) which, as mentioned above, is populated radiatively from $^2G(2)_{9/2}$, or to another Ln^{3+} impurity species.

Emission from $4f^25d$. The time-resolved spectrum, Figure 5, shows that emission is not only observed from $4f^3\ ^2G(2)_{9/2}\Gamma_{8u}$ but emission with a much shorter lifetime is also observed from $4f^25d$ to low energy of ∼52 630 cm^{-1}. The calculation of the $4f^25d$ energy levels referred to in Section 3 enables the assignment of the luminescent state to $(^3H)^4I_{9/2}\ \Gamma_{8g}$, with a small admixture of $^4K_{9/2}\ \Gamma_{8g}$. This level is almost 200 cm^{-1} below the next highest (Γ_{6g}) so that at low temperature (9 K) the higher energy levels are not appreciably populated. All transitions to $4f^3$ from Γ_{8g} are potentially electric dipole allowed under the site symmetry selection rules, although the free ion selection rules may impose restrictions. The calculated positions and relative emission intensities from this lowest $4f^25d$ energy level to the crystal field levels of $4f^3$ are shown as vertical bars in Figure 5, and it is clear that nearly all of the intensity resides in the transitions to the ^4I_J terminal multiplet term. This is in marked contrast to the emission from the $4f^3$ crystal field state

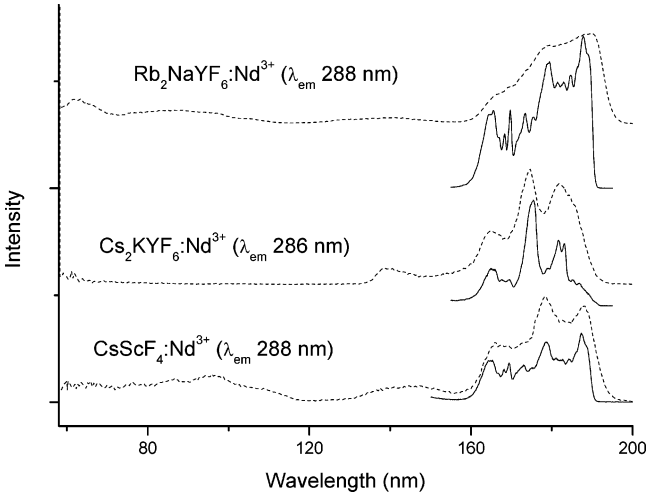

Figure 7. Excitation spectra of Nd^{3+} in fluoride hosts. The dashed (solid) curves are at room temperature (9 K) and are shifted vertically for clarity. The relative intensities are arbitrary.

$^2G(2)_{9/2}\Gamma_{8u}$ at ~4800 cm^{-1} to lower energy, where the transitions terminating upon ^4I_J are very weak.

Excitation Spectra. The intense $4f^3\ ^2G(2)_{9/2}\Gamma_{8u} \rightarrow 4f^3\ ^2F_{5/2}$ emission at 286−288 nm was monitored as a function of SR excitation wavelength, and the 9 K spectrum of $Cs_2NaYF_6:Nd^{3+}$ is shown in Figure 6a and b as the full line. Calculation shows that the $4f^25d$ levels extend from 52 630 cm^{-1} up to 128 054 cm^{-1} (i.e., ca. 190 nm up to 78 nm). The calculated positions and intensities of transitions from the $4f^3\ ^4I_{9/2}$ ground state to the $4f^25d$ crystal field levels are shown as vertical bars in these figures. Also, simulated vibronic spectra (as described in Section 3) are included. Note that only one progression forming mode (476 cm^{-1}) is included in the simulation, whereas the well-resolved $4f^N \rightarrow 4f^{N-1}5d$ absorption spectra of Ln^{3+} in hexachloroelpasolite lattices indicate that there are several progression-forming vibrational modes.[27] Nevertheless, the fine structure in the first group of $4f^25d$ bands between 160 and 190 nm is fairly well reproduced (Figure 6a). The fact that this is not the case for the higher energy group between 115 and 150 nm, Figure 6b, indicates that energy transfer from these levels to the luminescent $4f^3$ state is less effective. Figure 7 shows the room- and low-temperature excitation spectra of Nd^{3+} in the other fluoride hosts. Note that strong host absorption starts in these matrixes at $\lambda < 130$ nm, and the energy transfer from these hosts to Nd^{3+} is rather inefficient. Similar behavior was also observed in Pr^{3+}-doped Cs_2KYF_6. [17]

5. Conclusions

This study has presented d−f and f−f emission spectra, as well as f−d excitation spectra, for a series of Nd^{3+}-doped hexafluoroelpasolite lattices. In contrast to the corresponding $Cs_2NaYCl_6:Nd^{3+}$ system, where the $4f^3 \rightarrow 4f^25d$ absorption bands commence at ~47 000 cm^{-1} but no emission is observed from the lowest $4f^25d$ level, fast emission is observed in the present case. It is interesting to compare the structure of the present d−f emission with that for other Nd^{3+} systems. In the case of $YPO_4:Nd^{3+}$ most of the $4f^25d \rightarrow 4f^3$ intensity also lies within the transitions to the terminal ^4I_J multiplet terms,[2,3,5] in particular to $^4I_{9/2}$, although as in the case of $LiYF_4:Nd^{3+}$ the transitions terminating upon ^4F_J and ^4G_J are also clearly observed.[6] The present d−f spectra of $M_2AYF_6:Nd^{3+}$ more closely resemble that of $KYF_4:Nd^{3+}$ where the transitions terminating upon ^4I_J totally dominate the intensity profile. In all of these cases, the peak of the luminescence intensity lies in the region of ~180 to ~220 nm.

Not only is the occurrence of d−f emission a distinguishing factor between $Cs_2NaYF_6:Nd^{3+}$ and $Cs_2NaYCl_6:Nd^{3+}$, but the f−f emission characteristics also differ because of the higher phonon energies and faster internal conversion in the former system. Thus, emission is only expected from four $4f^3$ multiplet terms in $Cs_2NaYF_6:Nd^{3+}$, of which two have been reported in this study.

Acknowledgment. We thank the Hong Kong University Grants Commission for support of this study under the Research Grant CityU 102304. This work was also partly supported by the RFBR Grant 05-02-17306.

References and Notes

(1) van Pieterson, L.; Reid, M. F.; Wegh, R. T.; Meijerink, A. *J. Lumin.* **2001**, *94*−*95*, 79.
(2) Makhov, V. N.; Kirikova, N. Yu.; Kirm, M.; Krupa, J. C.; Liblik, P.; Lushchik, A.; Luschik, Ch.; Negodin, E.; Zimmerer, G. *Nucl. Instrum. Methods Phys. Res.* **2002**, *A486*, 437.
(3) Peijzel, P. S.; Vergeer, P.; Meijerink, A.; Reid, M. F.; Boatner, L. A.; Burdick, G. W. *Phys. Rev. B* **2005**, *71*, 045116.
(4) Wisniewski, D.; Tavernier, S.; Dorenbos, P.; Wisniewska, M.; Wojtowicz, A. J.; Bruyndonckx, P.; van Loef, E.; van Eijk, C. W. E.; Boatner, L. A. *IEEE Trans. Nucl. Sci.* **2002**, *49*, 937.
(5) Becker, J.; Gesland, J. Y.; Kirikova, N. Yu.; Krupa, J. C.; Makhov, V. N.; Runne, M.; Queffelec, M.; Uvarova, T. V.; Zimmerer, G. *J. Alloys Compd.* **1998**, *275*−*277*, 205.
(6) Lo, D.; Makhov, V. N.; Khaidukov, N. M.; Krupa, J. C.; Gesland, J. Y. *J. Lumin.* **2004**, *106*, 15.
(7) Khaidukov, N. M.; Kirm, M.; Lam, S. K.; Lo, D.; Makhov, V. N.; Zimmerer, G. *Opt. Commun.* **2000**, *184*, 183.
(8) Collombet, A.; Guyot, Y.; Joubert, M. F.; Laroche, M.; Margerie, J.; Moncorgé, R.; Descroix, E. *Phys. Rev. B* **2003**, *68*, 035115.
(9) Reid, M. F.; van Pieterson, L.; Wegh, R. T.; Meijerink, A. *Phys. Rev. B* **2000**, *62*, 14744.
(10) Collombet, A.; Guyot, Y.; Joubert, M. F.; Margerie, J.; Moncorgé, R. *Opt. Mater*. **2003**, *24*, 215.
(11) Zhou, X.; Tanner, P. A.; Faucher, M. D. *Phys. Rev. B* **2006**, *73*, 075113.
(12) Collombet, A.; Guyot, Y.; Mak, C. S. K.; Tanner, P. A.; Joubert, M. F. *J. Lumin.* **2001**, *94*−*95*, 39.
(13) Makhov, V. N.; Khaidukov, N. M.; Lo, D.; Krupa, J. C.; Kirm, M.; Negodin, E. *Opt. Mater.* **2005**, *27*, 1131.
(14) Ma, C.; Tanner, P. A.; Xia, S.; Yin, M. *Opt. Mater.*, in press, 2006.
(15) Aull, B. F.; Jenssen, H. P. *Phys. Rev. B* **1986**, *34*, 6640.
(16) Aull, B. F.; Jenssen, H. P. *Phys. Rev. B* **1986**, *34*, 6647.
(17) Schiffbauer, D.; Wickleder, C.; Meyer, G.; Kirm, M.; Stephan, M.; Schmidt, P. C. *Z. Anorg. Allg. Chem.* **2005**, *631*, 3045.
(18) Tanner, P. A.; Liu, Y. L.; Edelstein, N.; Murdoch, K.; Khaidukov, N. M. *J. Phys. Condens. Matter* **1997**, *9*, 7817.
(19) Meyer, G. *Prog. Solid State Chem.* **1982**, *14*, 141.
(20) Vtyurin, A. N.; Bulou, A.; Krylov, A. S.; Shmygol, I. V.; Aleksandrov, K. S. *J. Raman Spectrosc.* **2000**, *31*, 151.
(21) Zimmerer, G. *Nucl. Instr. Methods Phys. Res., Sect. A* **1991**, *308*, 178.
(22) Carnall, A. T.; Goodman, G. L.; Rajnak, K.; Rana, R. S. *J. Chem. Phys.* **1989**, *90*, 3443.
(23) (a) van Pieterson, L.; Reid, M. F.; Wegh, R. T.; Soverna, S.; Meijerink, A. *Phys. Rev. B* **2002**, *65*, 045113. (b) van Pieterson, L.; Reid, M. F.; Wegh, R. T.; Soverna, S.; Meijerink, A. *Phys. Rev. B* **2002**, *65*, 045114.
(24) Cowan, R. D. *The Theory of Atomic Structure and Spectra*; University of California, Berkeley, 1981.
(25) Denning, R. G. In *Vibronic Processes in Inorganic Chemistry*; Flint, C. D., Ed.; Kluwer: Dordrecht, 1989; Vol. 288, p 111.
(26) Ning, L.; Jiang, Y.; Xia, S.; Tanner, P. A. *J. Phys.: Condens. Matter* **2003**, *15*, 7337.
(27) Tanner, P. A. *Top. Curr. Chem.* **2004**, *241*, 167.
(28) Tanner, P. A. *Chem. Phys. Lett.* **1988**, *145*, 134.